




Towards Stable Free Lead Mixed Halide Perovskite Thin Films on FTO-Coated Glass Substrate

YOUSOUF DOUMBIA ^{1,4} AMAL BOUICH,^{1,3,5}
BERNABÉ MARI SOUCASE,¹ and DONAFOLOGO SORO²

1.—Institut de Disseny per a la Fabricació i Producció Automatitzada, Universitat Politècnica de València, 46022 Valencia, Spain. 2.—Département des Sciences et Technologie, Ecole Normale Supérieure (ENS) d'Abidjan, BP 10 Abidjan 08, Ivory Coast. 3.—Física Aplicada a las Ingenierías Aeronáutica y Naval & Instituto de Energía Solar, Universidad Politécnica de Madrid, 28040 Madrid, Spain. 4.—e-mail: doumbiayoussouf59@yahoo.fr. 5.—e-mail: bouich.amal@gmail.com

All-inorganic cesium (Cs) lead perovskites have better thermal and chemical stability than organic–inorganic hybrids. They therefore represent a hope for stability and increased performance of perovskites as absorber layers in photovoltaic solar cells. In the present work, we have deposited different layers on FTO-coated glass substrates using the one-step spin-coating method. The results of the lead substitution are presented and critically discussed. The X-ray diffraction (XRD) results show four peaks for all three samples. The main peaks of the different films are located at the 2θ angles of 26.45° and 51.50° for the Muller indices (220) and (242), respectively. These two main peaks indicate that the prepared thin films all have two preferred crystallographic orientations. Beyond these two main peaks, we have two other smaller peaks at 2θ of 33.67° and 37.70° corresponding to the Muller indices of (210) and (211), respectively. The smoother the surface of the thin films, the more light they reflect, resulting in poor light absorption by the films. It is therefore important to obtain a surface image of the prepared films, as the larger the surface image, the better the film. With this in mind, we carried out a scanning electron microscope (SEM) analysis, which gave us the surface images. Figure 3 shows the SEM images of thin $\text{CsPb}_{1-x}\text{Sn}_x\text{I}_{1.5}\text{Br}_{1.5}$ layers ($x = 0, 0.5$, and 1) grown on FTO-coated glass substrate with different [Pb]/[Sn] ratios. As can be seen from the figure, the effect of the [Pb]/[Sn] ratio is visible in the surface images of the different thin films. The smallest grain size is that of the unsubstituted $\text{CsPbI}_{1.5}\text{Br}_{1.5}$, while the largest grain size corresponds to the partially Pb-substituted layer ($\text{CsPb}_{0.5}\text{Sn}_{0.5}\text{I}_{1.5}\text{Br}_{1.5}$). The fully Pb-substituted layer ($\text{CsSnI}_{1.5}\text{Br}_{1.5}$) has an intermediate grain size. The surface images of the films show that the surfaces are well coated with grain sizes that vary greatly depending on the layer. The best grain size is that of the thin film with partial lead substitution ($\text{CsPb}_{0.5}\text{Sn}_{0.5}\text{I}_{1.5}\text{Br}_{1.5}$). Regarding the UV-visible absorption of the different films, we can say that the films absorb the maximum amount of light in the wavelength range of 350–550 nm. Above 550 nm, the absorption coefficients drop significantly. The absorption coefficients of the tin-free (Sn) layer remain higher than the coefficients of the other layers throughout the UV-visible spectrum. The degradation study revealed that the Sn-free layer retains good light absorption compared to the other layers after 4 weeks of exposure to the ambient environment. The crystal structure of all the layers shows good resistance to the elements during the 4 weeks, as shown by the renewed XRD results after the 4 weeks of exposure.

INTRODUCTION

Faced with the urgent need for a new solution to our mode of energy production and use due to environmental issues and the reserve of fossil resources, research is being carried out by scientists, much of which is directed toward the production of green energies, such as thermal, wind, and especially photovoltaic. Significant progress has been made in the last solution, and, thanks to this research, we have gone from first-generation photovoltaic cells composed of classic semiconductors to third-generation cells, i.e., thin layers. Photovoltaic perovskites have experienced a rapid explosion compared to other generations of cells. Perovskites are currently one of the most sought-after materials. They generally have the structure of ABX_3 -type with group A, either organic–inorganic hybrid or fully inorganic (methylammonium, formamidinium, cesium, ...), group B, a metal ion (Pb^{2+} , Sn^{2+} , ...), and a halogen or a halogen mix (iodine, chlorine, bromine, Br/I, Br/Cl, and I/Cl). The malleability of the perovskite structure gives several advantages, which have made perovskites the object of much research as an active layer in solar cells, since the synthesis of the first organic–inorganic hybrid lead halide cell in 2009.^{1–4} These halogenated perovskites have become one of the most important materials in the photovoltaic field due to their low cost and ease of production, which makes them promising candidates,^{5–8} conversion efficiency which quickly reached 25.5%,⁹ good charge carrier mobility,¹⁰ low effective exciton mass,¹¹ and structural defect tolerance.¹² However, lead halide perovskites are unstable and toxic due to the presence of lead,^{13–15} which limits the large-scale practical application of solar cells. Among all perovskites, all-inorganic cesium (Cs) perovskites have more advantages due to their relatively higher stability and balanced mobility compared to their organic–inorganic hybrid counterparts.¹⁶ Thus, several elements, such as tin (Sn), germanium (Ge), copper (Cu), bismuth (Bi), and antimony (Sb),^{17–21} have been proposed to overcome the toxicity problem of lead. Among all these options, tin (Sn^{2+}) is the most suitable ion for lead (Pb) substitution due to their equal valence and similar ionic radii (Sn^{2+} 1.35 Å and Pb^{2+} 1.49 Å.^{22,23} Point defects and other defects due to the presence of Sn, which are the likely sites of recombination, are removed by lead iodide (PbI_2).^{24–28} Beyond photovoltaics, perovskites contribute to the development of other technologies such as lasers, light-emitting diodes, etc. In this work, we have chosen the all-inorganic cesium perovskite, $CsPb_{1-x}Sn_xI_{1.5}Br_{1.5}$. The substitution of Pb by Sn in the mixed iodine–bromine cesium perovskite, $CsPb_{1-x}Sn_xI_{1.5}Br_{1.5}$ (with $x = 0; 0.5$ and 1), has been carried out to overcome the lead toxicity problem while improving the stability and performance of the thin films developed through the iodine–bromine (I/Br) mix in equal proportions.

MATERIALS AND METHODS

Experimental Details

The deposition of the $CsPb_{1-x}Sn_xI_{1.5}Br_{1.5}$ thin films was carried out using the one-step spin-coating method. The solutions to be deposited were obtained by dissolving the precursors, CsI, CsBr, SnI_2 , $SnBr_2$, PbI_2 , and $PbBr_2$, in dimethylformamide (DMF) and dimethylsulphoxide (DMSO) solvents. We first dissolved PbI_2 in DMF and then CsI for the $CsPb_{1.5}Br_{1.5}$ solution, and then SnI_2 again in DMF and CsI for the $CsPb_{1-x}Sn_xI_{1.5}Br_{1.5}$ and $CsSn_xI_{1.5}Br_{1.5}$ solutions. PbI_2 was dissolved in DMSO followed by CsBr for the $CsPb_{1-x}Sn_xI_{1.5}Br_{1.5}$ and $CsSn_xI_{1.5}Br_{1.5}$ solutions, and $SnBr_2$ in DMSO followed by CsBr for the $CsSn_xI_{1.5}Br_{1.5}$ solution.

The solutions were deposited on pre-treated fluoride-doped glass (FTO) substrates. Drops of iodidric acid (HI) and bromide acid (HBr) were added to promote better adhesion of the films to the substrate. We used toluene as an anti-solvent. Depositions were performed in a glovebox by spin-coating method with a speed of 4000 rpm in the 50 s, and the films were annealed at a temperature of 80 °C for 20 min. Figure 1 is the image summary of the deposition process of the different inorganic $CsPb_{1-x}Sn_xI_{1.5}Br_{1.5}$ films that we developed.

Characterization of Thin Films

The study of thin films can only be completed by carrying out various characterizations. These analyses allow us to obtain the properties of the films:

- X-ray diffraction (XRD; Ultima IV; RIGAKU) was used to obtain the crystal structure of the thin films, taking the angle range from 10° to 60° with CuK α radiation ($\lambda = 1.54$ Å) at room temperature.
- The characteristic surface morphology of the thin films was analyzed by scanning electron microscopy (SEM; 200-FEI; Quanta) under a potential of 1.5 kV.
- In addition, UV-visible spectra were obtained with a HR4000 spectrophotometer (Ocean Optics) in the range of 300–900 nm to give us the optical properties of the thin films.

RESULTS AND DISCUSSION

X-ray Diffraction Analyses

In the present work, $CsPb_{1-x}Sn_xI_{1.5}Br_{1.5}$ perovskite thin films ($x = 0, 0.5$, and 1) were successfully deposited on FTO-coated glass substrates using the one-step spin-coating method. Figure 1a shows the results of the XRD analysis of the thin films. The different peaks located at 26.45°, 33.67°, 37.70°, and 51.50° correspond to the (220), (210), (211), and (242) crystallographic planes, respectively, in agreement with the structure of the mixed I/Br perovskite in Cs. The main peaks of the

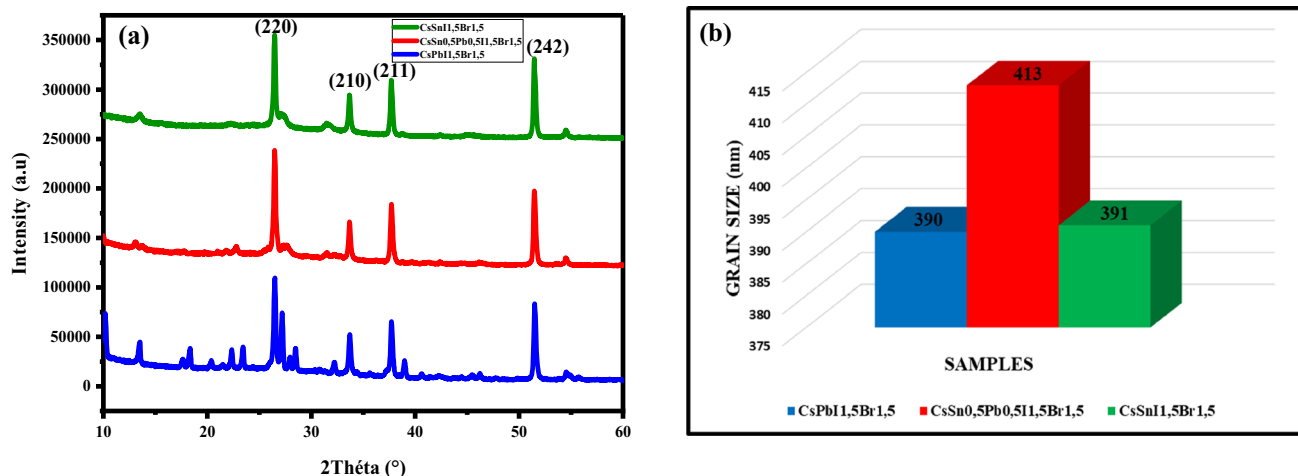


Fig 1. XRD of 50:50 iodine–bromine mixed halide thin films with lead substitution (a) and grain size (b).

different films are located at the 2θ angles of 26.45° and 51.50° for the Miller indices (220) and (242), respectively. These two main peaks indicate that the prepared thin films have two preferred crystallographic orientations. Beyond these two main peaks, we have two other smaller peaks at 2θ of 33.67° and 37.70° corresponding to the Miller indices of (210) and (211), respectively. A slight increase in the peaks is observed in the case of the total substitution of Pb by Sn and a slightly larger increase for partial substitution of Pb, which is in line with the grain size as given in Fig. 1b. The lack of a shift of the peaks to larger or smaller 2θ angles in the partial and total substitution layers, compared to the peaks in the layer without Pb substitution, indicates not only that there is no interstitial position but also that the ionic radii of lead (Pb^{2+}) and tin (Sn^{2+}) are indeed similar.²² There is therefore no structural deformation. The incorporation of Sn limits the tendency for peak splitting, giving the films a single-phase structure. Through the analysis of the crystal structure of the layers, we can say that all the layers have the same perovskite phase, which is in line with the results found in the literature.^{29,30} Furthermore, the maximum width at mid-height of the peaks (220) shows an improvement in crystallinity when Sn is added, and the best crystallinity is that of the partially substituted layer ($\text{CsPb}_{1-x}\text{Sn}_x\text{I}_{1.5}\text{Br}_{1.5}$).

Scanning Microscopic Analysis (SEM)

The analysis of the surface morphology of photovoltaic thin films is very important. The smoother the surface of the thin film, the more it reflects light, which results in poor light absorption by the film. It is therefore important to obtain a surface image of the prepared films. The larger the surface image, the better the film. With this in mind, we carried out a SEM analysis which gave us the surface images shown in Fig. 2 of the $\text{CsPb}_{1-x}\text{Sn}_x\text{I}_{1.5}\text{Br}_{1.5}$ ($x = 0, 0.5$

and 1) thin films grown on FTO substrates with different [Pb]/[Sn] ratios. As can be seen from the figure, the effect of the [Pb]/[Sn] ratio is visible in the surface images of the different thin films. The smallest grain size is that of the unsubstituted $\text{CsPbI}_{1.5}\text{Br}_{1.5}$, while the largest grain size corresponds to the partially Pb-substituted layer ($\text{CsPb}_{0.5}\text{Sn}_{0.5}\text{I}_{1.5}\text{Br}_{1.5}$). The fully Pb-substituted layer ($\text{CsSnI}_{1.5}\text{Br}_{1.5}$) has an intermediate grain size. This improvement in grain size may be due to the crystal growth decreasing crystal nucleation and leading to higher crystallinity,^{31,32} and a decrease in trap state defects which favors the decrease in non-radiative recombination at the surface.^{33,34} This grain size order was confirmed by the XRD results (Fig. 1b). However, it should be noted that the best layer in terms of grain size is obtained for moderate Sn incorporation, which is consistent with the results found in the literature.^{35–37} The surface images of the $\text{CsPb}_{0.5}\text{Sn}_{0.5}\text{I}_{1.5}\text{Br}_{1.5}$ and $\text{CsPbI}_{1.5}\text{Br}_{1.5}$ thin films show well-coated surfaces with no holes, voids, or cracks, whereas that of $\text{CsSnI}_{1.5}\text{Br}_{1.5}$ shows voids.

Analysis of Optical Properties

Optical absorption measurements of the thin films were carried out to analyze their optical properties. Figure 3a shows the optical coefficients over the visible spectrum from 300 nm to 900 nm wavelength. All the thin films have their absorption maxima between about 350 nm and 500 nm. The layer without Pb substitution has higher absorption coefficients than the layers with partial and total Sn substitution. The partially doped layer has an average absorption. When we look at the band gap, we can see that the layer with total substitution of Pb by Sn is more likely to generate excitons more easily, while the layer with partial substitution generates electron–hole pairs with more difficulty. This shows once again that it is not enough to

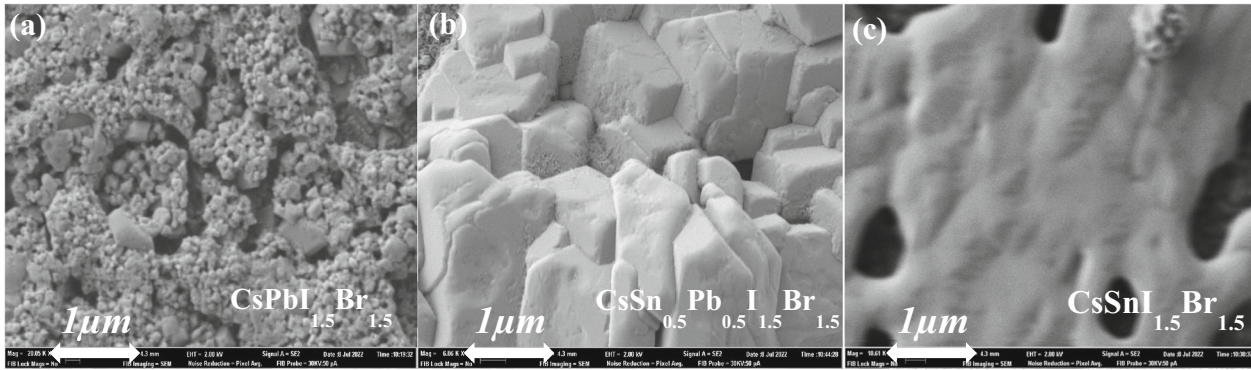


Fig 2. SEM surface images of iodine–bromine mixed halide thin films with a magnification of 1 μm with 50:50 lead substitution: (a) CsPbI_{1.5}Br_{1.5}, (b) CsSn_{0.5}Pb_{1.5}Br_{1.5}, and (c) CsSnI_{1.5}Br_{1.5}.

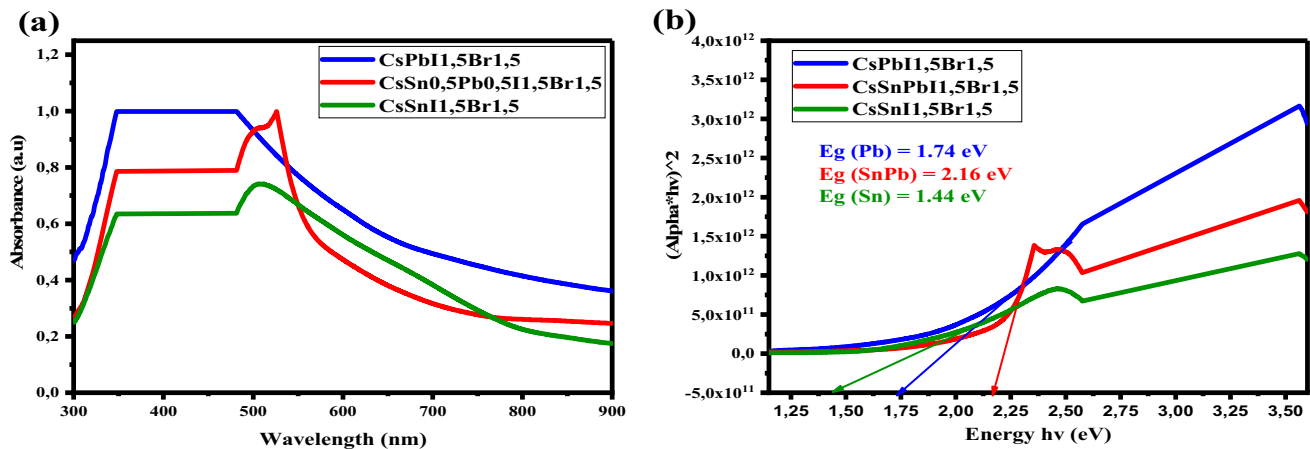


Fig 3. (a) Absorption of iodine–bromine mixed halide thin films with 50:50 lead substitution, (b) band gap.

absorb more photons, but that the photons must have the necessary energy to create the electron–hole pairs. The band gaps are located between 1.44 eV and 2.16 eV, as shown in Fig. 3b. We can say that the mixing of iodine–bromine (I_{1.5}/Br_{1.5}) and the incorporation of Sn have allowed the reducing of the band gap to intermediate values, and that the band gap of CsPbI₃ is about 1.74 eV and that of CsPbBr₃ is 2.27 eV.^{16,38}

DEGRADATION STUDY

One of the major problems of perovskites is their vulnerability to oxygen and moisture.^{39–44} Thus, perovskites degrade more rapidly when exposed to the ambient environment, causing their structural instability. In this study, we incorporated Sn to overcome the Pb toxicity problem and the rapid degradation of CsPb_{1-x}Sn_xI_{1.5}Br_{1.5} perovskites ($x = 0, 0.5, \text{ and } 1$). The samples were prepared on an FTO-coated glass substrate using the one-step spin-coating method. After the various analyses of the fresh samples, they were stored in the ambient environment for 4 weeks.

In Fig. 4, the x-ray diffraction results after 4 weeks are compared with the results of the fresh samples. We can see from Fig. 4a showing 0% Sn, Fig. 4b showing 50% Sn, and Fig. 4c showing 100% Sn in substitution of Pb that there is no significant decrease in the diffraction peaks. Therefore, we can confirm from a structural point of view that Sn has improved the stability of the different samples [45–54].

In Fig. 5, we can see a moderate decrease in the absorption coefficients of the 0% Sn sample (Fig. 5a), while the decrease is a little larger for the 50% Sn and 100% Sn samples (Fig. 5b and c, respectively). These decreases in the absorption coefficients demonstrate the degradation of the samples following exposure to the ambient environment. After 4 weeks in the ambient environment, the optical properties of the samples deteriorate. However, it should be noted that the 0% Sn layer (CsPbI_{1.5}Br_{1.5}) is more resistant than the layers containing Sn (CsPb_{0.5}Sn_{0.5}I_{1.5}Br_{1.5} and CsSnI_{1.5}Br_{1.5}) in terms of their optical properties.

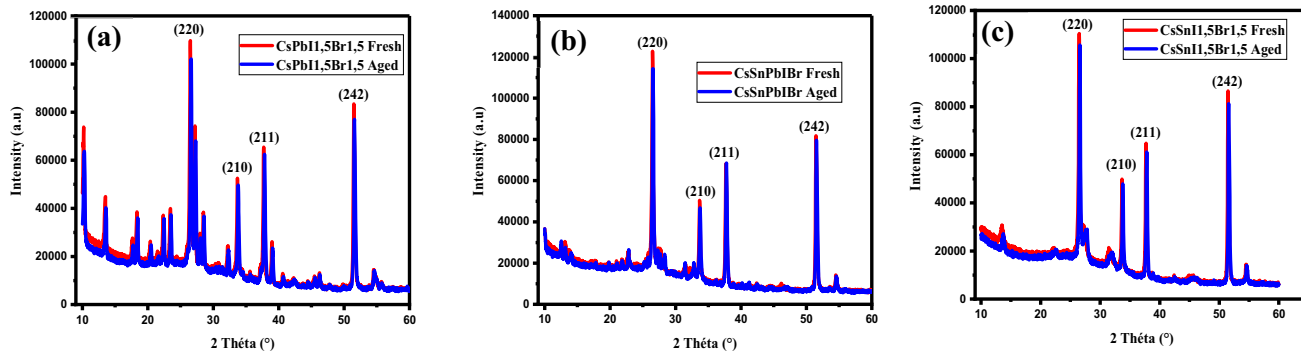


Fig 4. XRD patterns of fresh Sn-substituted mixed halide iodine/lead perovskite aged after 4 weeks in dark conditions at 22% humidity: (a) $\text{CsPb}_{1.5}\text{Br}_{1.5}$, (b) $\text{CsSn}_{0.5}\text{Pb}_{1.5}\text{Br}_{1.5}$, and (c) $\text{CsSn}_{1.5}\text{Br}_{1.5}$.

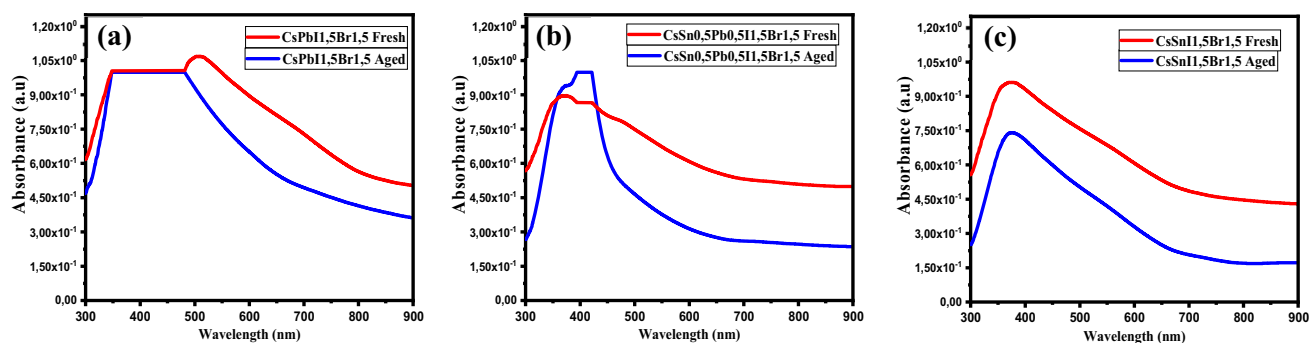


Fig 5. Absorption spectra of Sn-substituted mixed iodine/lead bromide perovskite fresh and aged after 4 weeks under dark conditions at 22% humidity: (a) $\text{CsPb}_{1.5}\text{Br}_{1.5}$, (b) $\text{CsSn}_{0.5}\text{Pb}_{1.5}\text{Br}_{1.5}$, and (c) $\text{CsSn}_{1.5}\text{Br}_{1.5}$.

CONCLUSION

We obtained well-crystallized $\text{CsPb}_{1-x}\text{Sn}_x\text{I}_{1.5}\text{Br}_{1.5}$ perovskite thin films from the one-step spin-coating method. The crystallographic features were analyzed using x-ray diffraction over a range of 10–60° with the diffraction angle 2θ . This analysis showed us an enhancement of the crystal structure of the thin films containing tin. There was no deformation of the crystal structure of the different thin films, due to the similarity of the ionic radii of Pb^{2+} and Sn^{2+} . Regarding the surface morphology of the layers, we observed an improvement in the grain size when tin was incorporated. The thin films are well-coated and dense. The optical properties of our different thin films showed good light absorption in the UV-visible range as well as an improvement of the band gap compared to CsPbI_3 and CsPbBr_3 films. As for the stability of the layers over time, it must be said that the layers resist the degradation of the crystalline structure, since the peaks of the aged layers did not show a decrease compared to those of the fresh layers. The absorption coefficients showed a decrease for the aged films and thus indicated a degradation of the optical properties of the layers. It should be noted that the different thin layers were each reproduced 3 times with a margin of error of about 4%.

ACKNOWLEDGEMENTS

Author Youssef Dombia acknowledges his grant from Erasmus+ KA 107. The author Amal Bouich acknowledges MCIN for funding support through Margarita Salas Fellowship (MCIN/AEI/10.13039/501100011033). The Postdoctoral contract Margarita Salas financed with the union European Next Generation EU. This research has been funded by Grant PID2019-107137RB-C22 funded by MCIN/AEI/ and by “ERDF A way of making Europe”.

FUNDING

Open Access funding provided thanks to the CRUE-CSIC agreement with Springer Nature.

CONFLICT OF INTEREST

The authors declare that they have no conflict of interest.

OPEN ACCESS

This article is licensed under a Creative Commons Attribution 4.0 International License, which permits use, sharing, adaptation, distribution and reproduction in any medium or format, as long as you give appropriate credit to the original author(s) and the source, provide a link to the Creative

Commons licence, and indicate if changes were made. The images or other third party material in this article are included in the article's Creative Commons licence, unless indicated otherwise in a credit line to the material. If material is not included in the article's Creative Commons licence and your intended use is not permitted by statutory regulation or exceeds the permitted use, you will need to obtain permission directly from the copyright holder. To view a copy of this licence, visit <http://creativecommons.org/licenses/by/4.0/>.

REFERENCES

1. A. Kojima, K. Teshima, Y. Shirai, and T. Miyasaka, *J. Am. Chem. Soc.* 131(17), 6050 (2009).
2. H.H. Fang, R. Raissa, M. Abdu-Aguye, S. Adjokatse, G.R. Blake, J. Even, and M.A. Loi, *Adv. Func. Mater.* 25(16), 2378 (2015).
3. Y. Zhao, and K. Zhu, *Chem. Soc. Rev.* 45(3), 655 (2016).
4. U. Khan, Y. Zhinong, A.A. Khan, and A. Zulfiqar, *Sol. Energy* 189, 421 (2019).
5. B.R. Sutherland, and E.H. Sargent, *Nat. Photonics* 10(5), 295 (2016).
6. L.N. Quan, F.P. García de Arquer, R.P. Sabatini, and E.H. Sargent, *Adv. Mater.* 30(45), 1801996 (2018).
7. Y. Fu, H. Zhu, J. Chen, M.P. Hautzinger, X.Y. Zhu, and S. Jin, *Nat. Rev. Mater.* 4(3), 169 (2019).
8. Cho, H., Jeong, S. H., Park, M. H., Kim, Y. H., Wolf, C., Lee, C. L., & Sadhanala, A. NoS. Myoung, S. Yoo, SH Im, RH Friend, and T.-W. Lee. *Science*, 350(5), (2015).
9. Wu, T., Qin, Z., Wang, Y., Wu, Y., Chen, W., Zhang, S., Cai, M., Dai, S., Zhang, J., Liu, J., et al. *Nano-Micro Lett*, 13, 152. [CrossRef] [PubMed], (2021).
10. D. Stranks, E. Eperon, G. Grancini, C. Menelaou, J. Alcocer, T. Leijtens, and J. Snaith, *Science* 342, 341–344 (2013).
11. T. Wang, B. Daiber, J.M. Frost, S.A. Mann, E.C. Garnett, A. Walsh, and B. Ehrler, *Energy Environ. Sci.* 10(2), 509–515 (2017).
12. H. Huang, M.I. Bodnarchuk, S.V. Kershaw, M.V. Kovalenko, and A.L. Rogach, *ACS Energy Lett.* 2(9), 2071 (2017).
13. W. Lv, X. Tang, L. Li, L. Xu, M. Li, R. Chen, and W. Huang, *J. Phys. Chem. C* 123(39), 24313 (2019).
14. H. Cho, Y.H. Kim, C. Wolf, H.D. Lee, and T.W. Lee, *Adv. Mater.* 30(42), 1704587 (2018).
15. M.A. Kamarudin, D. Hirotani, Z. Wang, K. Hamada, K. Nishimura, Q. Shen, and S. Hayase, *The journal of physical chemistry letters* 10(17), 5277 (2019).
16. C.A. López, C. Abia, M.C. Alvarez-Galván, B.K. Hong, M.V. Martínez-Huerta, F. Serrano-Sánchez, and J.A. Alonso, *ACS Omega* 5(11), 5931 (2020).
17. Z. Zhang, L. Wang, A.K. Baranwal, S.R. Sahamir, G. Kapil, Y. Sanehira, and S. Hayase, *J. Energy Chem.* 71, 604 (2022).
18. A. Toshniwal, and V. Kheraj, *Sol. Energy* 149, 54 (2017).
19. Abate, A. (2017). *Joule*, 1(4), 659-664, (2017).
20. F. De Angelis, *ACS Energy Lett.* 6(4), 1586 (2021).
21. W. Ke, and M.G. Kanatzidis, *Nat. Commun.* 10(1), 1 (2019).
22. E.W.G. Diau, E. Jokar, and M. Rameez, *ACS Energy Lett.* 4(8), 1930 (2019).
23. Z. Zhang, A. Kumar Baranwal, S. Razey Sahamir, G. Kapil, Y. Sanehira, M. Chen, and S. Hayase, *Solar RRL* 5(11), 2100633 (2021).
24. E. Aydin, M. De Bastiani, and S. De Wolf, *Adv. Mater.* 31(25), 1900428 (2019).
25. T.H. Chowdhury, R. Kaneko, T. Kaneko, K. Sodeyama, J.J. Lee, and A. Islam, *Chem. Eng. J.* 431, 133745 (2022).
26. T.A. Berhe, W.N. Su, C.H. Chen, C.J. Pan, J.H. Cheng, H.M. Chen, and B.J. Hwang, *Energy Environ. Sci.* 9(2), 323 (2016).
27. S. Akin, Y. Altintas, E. Mutlugun, and S. Sonmezoglu, *Nano Energy* 60, 557 (2019).
28. El Mouden, A., El Messaoudi, N., El Guerraf, A., Bouich, A., Mehmeti, V., Lacherai, A., & Sher, F. *Chemosphere*, 137922. (2023).
29. S. Wang, Y. Jiang, E.J. Juarez-Perez, L.K. Ono, and Y. Qi, *Energie naturelle* 2(1), 1 (2016).
30. Q. Chen, H. Zhou, T.B. Song, S. Luo, Z. Hong, H.S. Duan, and Y. Yang, *J. Cryst. Growth* 360, 68 (2012).
31. W. Chen, H. Chen, G. Xu, R. Xue, S. Wang, Y. Li, and Y. Li, *Joule* 3(1), 191 (2019).
32. C.W. Lan, W.C. Lan, T.F. Lee, A. Yu, Y.M. Yang, W.C. Hsu, and A. Yang, *J. Cryst. Growth* 360, 68 (2012).
33. M. Gerhard, B. Louis, R. Camacho, A. Merdasa, J. Li, A. Kiligariadis, and I.G. Scheblykin, *Nat. Commun.* 10(1), 1 (2019).
34. D.A. Kara, D. Cirak, and B. Gultekin, *Phys. Chem. Chem. Phys.* 24(17), 10384 (2022).
35. M. Schaefer, R.A. Fournelle, and J. Liang, *J. Electron. Mater.* 27, 1167 (1998).
36. Abdel-Shakour, M., Chowdhury, T. H., Matsuishi, K., Bedja, I., Moritomo, Y., & Islam, A. *Solar rrl*, 5(1), 2000606. (2021).
37. J. Zhang, G. Hodes, Z. Jin, and S. Liu, *Angewandte Chemie Int. Edn.* 58(44), 15596 (2019).
38. N. Parikh, M.M. Tavakoli, M. Pandey, A. Kalam, D. Prochowicz, and P. Yadav, *Sustain. Energy Fuels* 5(5), 1255 (2021).
39. H.B. Lee, N. Kumar, B. Tyagi, S. He, R. Sahani, and J.W. Kang, *Mater. Today Energy* 21, 100759 (2021).
40. A. Bouich, B. Mari, L. Atourki, S. Ullah, and M.E. Touhami, *Jom* 73(2), 551 (2021).
41. A. Uddin, M.B. Upama, H. Yi, and L. Duan, *Coatings* 9(2), 65 (2019).
42. S. Wang, Y. Jiang, E.J. Juarez-Perez, L.K. Ono, and Y. Qi, *Nat. Energy* 2(1), 1 (2016).
43. G. Niu, X. Guo, and L. Wang, *J. Mater. Chem. A* 3(17), 8970 (2015).
44. M.I. Asghar, J. Zhang, H. Wang, and P.D. Lund, *Renew. Sustain. Energy Rev.* 77, 131 (2017).
45. A. Bouich, Study and characterization of hybrid perovskites and copper-indiumgallium selenide thin films for tandem solar cells (Doctoral dissertation, Universitat Politècnica de València) (2021). <https://doi.org/10.4995/Thesis/10251/160621>.
46. A. Bouich, J. Mari-Guaita, B. M.Soucase, and P. Palacios, *Nanomaterials* 12(17), 2901 (2022).
47. J. Mari-Guaita, A.Bouich, and B. Mari, *Eng. Proc.* 12(1), 1 (2021).
48. N. El Messaoudi, A. El Mouden, Y. Fernine, M. El Khomri, A. Bouich, N. Faska, ... and A. Lacherai, *Environ. Sci. Pollut. Res.* 1–18 (2022).
49. A. Bouich, S. Ullah, H. Ullah, B. Mari, B. Hartiti, M. Ebn Touhami, and D. M. F. Santos, *Mater. Electron.* 30, 20832–20839 (2019).
50. S. Bouazizi, A. Bouich, W. Tlili, M. Amlouk, A. Omri, and B. M. Soucase, *J. Mol. Graph. Model.* 122, 108458 (2023).
51. Y. Doumbia, A. Bouich, D. Soro, and B. M. Soucase, *Optik*. 261, 169222 (2022).
52. S. Bouazizi, W. Tlili, A. Bouich, B. M. Soucase, and A. Omri, *Mater. Res. Express.* 9(9), 096402 (2022).
53. A. Bouich, J. Mari-Guaita, B. M. Soucase, and P. Palacios, *P. Mater. Res. Bull.* 163, 112213 (2023).
54. A. Bouich, J. C. Torres, H. Chfii, J. Mari-Guaita, Y. H. Khattak, F. Baig, ... and P. Palacios, *Sol. Energy* 250, 18–32 (2023).

Publisher's Note Springer Nature remains neutral with regard to jurisdictional claims in published maps and institutional affiliations.